Offset-Free Robust Adaptive Back-Stepping Speed Control for Uncertain Permanent Magnet Synchronous Motor

Seok-Kyoon Kim, June-Seok Lee, *Member, IEEE*, and Kyo-Beum Lee, *Senior Member, IEEE*

***Abstract*—This paper proposes a speed-control law for a parametrically uncertain surface-mounted permanent magnet synchronous motor (SPMSM) using a multivariable approach, which robustly and optimally stabilizes the tracking error dynamics using only the lower and upper bounds of the SPMSM parameters. The contributions of this article are twofold. First, both the inner- and outer-loop controllers are designed using a multivariable approach; the back-stepping controller design method ensures stability and the offset-free property. Second, it is shown that it is possible to systematically assign the robust global stabilizing control gains by solving an optimization problem. The efficacy of the proposed method is experimentally verified using a 3-kW SPMSM.**

***Index Terms*—Parametric uncertainty, permanent magnet synchronous motor (PMSM), robust speed tracking control, stability.**

I. Introduction

BECAUSE of their high efficiency, power factor, and density, permanent magnet synchronous motors (PMSMs) have been considered as an alternative to traditional dc and induction motors in many industrial applications [1]–[6].

Conventionally, it has been preferred to use the cascade speed control strategy for designing the speed controller of the PMSM. The cascade speed controller is comprised of the inner-loop current controller and the outer-loop speed controller in a cascade manner. Although both the inner and outer loop are designed to stabilize their desired error dynamics, respectively, it is questionable that the whole closed-loop system (combining the inner loop and outer loop) is also stable, which is a fundamental limitation of the cascade control scheme. In order to overcome this obstacle, recently, a multivariable approach has been introduced, which is based on the nonlinear control strategies such as the sliding mode control (SMC), model predictive control (MPC), fuzzy control, adaptive control methods, etc.

The proportional-integral (PI) controller was mainly utilized to control the inner and outer loop because of its simplicity [7], [8]. The PI gains were determined to meet the desired closed-loop performance in the frequency domain, and the additional feed-forward (F/F) compensation terms were introduced to improve the current transient performance. To improve the closed-loop performance in the time domain, various novel controllers such as the deadbeat method [9] and the feedback linearizing method [10], [11] for the inner loop have been developed. A robust control scheme [12] has been developed for the inner loop to improve the closed-loop robustness, employing the convergent state estimates of the disturbance observer. It is, however, questionable that these control schemes can maintain satisfactory closed-loop performance under parameter variations. To maintain satisfactory closed-loop performance, regardless of the disturbance caused by parameter variations and external noise, SMC scheme [13] has been devised for replacing the inner-loop PI controller, and there was another speed control algorithm [14] based on the SMC method through the multivariable approach. The optimal time-domain performance of their closed-loop system, however, should be found by tuning the control gain using the trial-and-error method because there has been no systematic way to assign the optimal control gain. It has been reported that the recent MPC methods in [15] and [16] provides a faster transient performance than the existing methods with the closed-loop optimality in some sense. However, there has been no proof that closed-loop systems controlled by the MPC method remains optimal in the presence of parameter uncertainties. There have been several fuzzy logic controllers [17], [18], adaptive speed controller [19], and back-stepping controllers [1], [20]–[25] based on the multivariable approach. Fuzzy logic control schemes [17], [18] consider all parameter uncertainties; however, the closed-loop stability has been proven only under the assumption that the control input is bounded at all times, and these schemes might require a heavy online computational effort. Although the adaptive speed-control law suggested in [19] considers all parametric uncertainties of the PMSM, it requires feedback regarding the accelerated speed, which is hard to access in practice. The adaptive back-stepping speed-control scheme in [1] guarantees that the PMSM speed follows its reference, estimating the resistance, mechanical friction, and load torque online; however, this controller needs to know the true values of inductance and flux, and its control gains should be tuned for a satisfactory closed-loop performance through a trial-error method. Although the other adaptive back-stepping methods presented in [20] and [21] handles the uncertainties of the all parameters, there was no systematic way of determining the optimal closed-loop performance. In particular, the recent

Manuscript received June 15, 2015; revised August 30, 2015; accepted December 2, 2015. Date of publication December 11, 2015; date of current version May 20, 2016. This work was supported by the Basic Science Research Program through the National Research Foundation of Korea funded by the Ministry of Education (2013R1A1A2A10006090). Recommended for publication by Associate Editor G. Escobar.

S.-K. Kim is with the Vehicle Component Technology Center, LG Electronics, Seoul 08592, Korea (e-mail: lotus45kr@gmail.com).

J.-S. Lee is with the Railroad Safety Research Division, Korea Railroad Research Institute, Uiwang, Seoul 16105, Korea (e-mail: ljs@krri.re.kr).

K.-B. Lee is with the Department of Electrical and Computer Engineering, Ajou University, Suwon 16499, Korea (e-mail: kyl@ajou.ac.kr).

Color versions of one or more of the figures in this paper are available online at http://ieeexplore.ieee.org.

Digital Object Identifier 10.1109/TPEL.2015.2508041

adaptive back-stepping method in [21] presented a method to avoid the singularity problem while estimating all of the electrical and mechanical parameters; this method attempted to enhance the closed-loop robustness against load torque using the sigma-modification terms for both the integrator and the adaptation law. However, there was no guarantee that the offset errors in the tracking errors are removed. The rest of the back-stepping methods [22]–[25] did not only consider the parameter variation of the inductance value but also offer any optimal method to determine the control gains.

This article presents an adaptive back-stepping speed controller design method for an surface-mounted PMSM (SPMSM) via the multivariable approach in the presence of parametric uncertainties, compensating for the inadequacies of the aforementioned methods in the literature. The proposed method has the same benefits in the result [21], and, in particular, the contrasts to previous result of [21] are divided into two parts: 1) the offset-free property is guaranteed thanks to consider the vector form of the PMSM dynamics instead of the scalar form, 2) an optimal control gain can be determined by solving an optimization problem under bilinear matrix inequality constraints, which robustly stabilizes the closed-loop system despite the parameter variations. The experimental results using a 3-kW SPMSM show that the proposed method significantly enhances the closed-loop performance relative to the classical cascade PI scheme.

II. SPMSM Model in Synchronous Rotating d-q Frame

In the synchronous rotating dq frame, the dynamics of the SPMSM are described as follows [1]:

$$\frac{di_d(t)}{dt} = -\frac{R_s}{L}i_d(t) + P\omega(t)i_q(t) + \frac{1}{L}u_d(t), \tag{1}$$

$$\frac{di_q(t)}{dt} = -P\omega(t)i_d(t) - \frac{R_s}{L}i_q(t) - \frac{P\lambda_m}{L}\omega(t) + \frac{1}{L}u_q(t), \tag{2}$$

$$\frac{d\omega(t)}{dt} = -\frac{B}{J}\omega(t) + \frac{1}{J}\Big(T_e(i_q(t)) - T_L(t)\Big), \quad \forall t \geq 0 \tag{3}$$

where $i_d(t)$, $i_q(t)$, and $\omega(t)$ denote the d-frame current, the q-frame current, and the rotor speed, respectively. The dq-frame input voltages are denoted by $u_d(t)$ and $u_q(t)$, respectively, which are treated as the control inputs. The electrical torque $T_e(i_q(t))$ is given by

$$T_e(i_q(t)) := \frac{3}{2}P\lambda_m i_q(t), \ \forall t. \tag{4}$$

The electrical coefficients R_s, L, and λ_m represent the stator resistance, inductance, and magnet flux, respectively. The mechanical coefficients B, J, and P denote the viscous friction, rotor moment of inertia, and the number of pole pairs, respectively. $T_L(t)$ refers to the load torque. R_s and L are the stator resistance and inductance, respectively. λ_m is the permanent magnet flux.

Note that it is difficult to always know the exact values of the electrical and mechanical parameters, except for the number of pole pairs P, because these values vary as the operating conditions change (e.g., the reference speed and the temperature). Moreover, the load torque $T_L(t)$ can also be abruptly changed by an unexpected load failure. Thus, in the rest of the paper, it is assumed that

1) All of the electrical and mechanical coefficients, except for the number of pole pairs P, are unknown, but the upper and lower bounds of these parameters are known, i.e., there exist known positive constants $R_{s,\min}$, $R_{s,\max}$, $L_{\min}$, $L_{\max}$, $\lambda_{m,\min}$, $\lambda_{m,\max}$, $B_{\min}$, $B_{\max}$, $J_{\min}$, and $J_{\max}$, such that

$$\begin{aligned} &0 < R_{s,\min} \leq R_s \leq R_{s,\max}, \quad 0 < L_{\min} \leq L \leq L_{\max}, \\ &0 < \lambda_{m,\min} \leq \lambda_m \leq \lambda_{m,\max}, \quad 0 < B_{\min} \leq B \leq B_{\max}, \\ &0 < J_{\min} \leq J \leq J_{\max}. \end{aligned} \tag{5}$$

2) The load torque $T_L(t)$ is unknown, but it can be decomposed as the sum of its dc component $T_{L,0}$ and its bounded time-varying component $\Delta T_L(t)$, i.e.,

$$T_L(t) = T_{L,0} + \Delta T_L(t), \ \forall t \tag{6}$$

where $|\Delta T_L(t)| \leq \beta$, $\forall t$, for some positive constant β.

3) The a-b-c (stationary) frame current, the SPMSM speed, and the corresponding d-q frame current are accessible for measurement.

Under these assumptions, a robust speed tracking control scheme is designed in the following section using the state equation comprised of (1), (2), and (3).

III. Speed Controller Design

In this section, a robust speed tracking control law is developed for attaining the following control objective:

$$\lim_{t\to\infty}\omega(t) = \omega_{\text{ref}} \text{ and } \lim_{t\to\infty} i_d(t) = i_{d,\text{ref}} \tag{7}$$

for a given constant speed reference ω_{ref} and d-frame current reference $i_{d,\text{ref}}$ under parametric uncertainties. Note that the current reference $i_{d,\text{ref}}$ is given for a maximized value of the torque-per-ampere within the rating speed operations; it is set to zero in the case of an SPMSM [26], [27]. On the other hand, in high-speed operation, $i_{d,\text{ref}}$ is determined such that the steady-state value of the control input is feasible, which is called field-weakening control. In this study, it is assumed that the d-frame reference $i_{d,\text{ref}}$ is set to zero.

First, because the load torque $T_L(t)$ acts as a mismatched, unknown disturbance in the speed dynamics (3), define the coordinate transformation as

$$e_{iq}(t) := i_q(t) - i_{q,\text{ref}}(t), \ \forall t \geq 0 \tag{8}$$

with $i_{q,\text{ref}}(t)$ being the virtual control input acting as the q-frame current reference to be designed later. Defining the speed tracking error as $e_\omega(t) := \omega(t) - \omega_{\text{ref}}$, $\forall t \geq 0$, with the speed

reference ω_{ref}, and using the dynamic (1), it follows that:

$$\begin{aligned} c_1\dot{e}_\omega(t) =& -c_2 e_\omega(t) + e_{iq}(t) + i_{q,\text{ref}}(t) + p_\omega \\ &+ w_{1,0} + w_1(t), \qquad (9) \\ \dot{e}_{iq}(t) =& \dot{i}_q(t) - \dot{i}_{q,\text{ref}}(t) \\ =& -P\omega(t) i_d(t) - \frac{R_s}{L} i_q(t) - \frac{P\lambda_m}{L}\omega(t) \\ &+ \frac{1}{L} u_q(t) - \dot{i}_{q,\text{ref}}(t),\ \forall t \geq 0 \qquad (10) \end{aligned}$$

where the unknown positive constants c_1, c_2, and p_ω are defined by

$$c_1 := \frac{2J}{3P\lambda_m},\ c_2 := \frac{2B}{3P\lambda_m},\ p_\omega := -\frac{2B\omega_{\text{ref}}}{3P\lambda_m}.$$

The disturbance signals $w_{1,0}$, $w_1(t)$ are defined as

$$w_{1,0} := -\frac{2T_{L,0}}{3P\lambda_m},\ w_1(t) := -\frac{2\Delta T_L(t)}{3P\lambda_m},\ \forall t \geq 0.$$

To stabilize the speed error dynamics (9), the virtual control input $i_{q,\text{ref}}(t)$ is chosen as

$$\begin{aligned} i_{q,\text{ref}}(t) =& -k_{P,\omega} e_\omega(t) - k_{I,\omega} z_\omega(t) \qquad (11) \\ \dot{z}_\omega(t) =& e_\omega(t),\ \forall t \geq 0 \qquad (12) \end{aligned}$$

where $k_{P,\omega}$ and $k_{I,\omega}$ represent the control gains, respectively.

Now, substituting the virtual control input (11) and (12) into the speed tracking error dynamics (9), we define the d-frame current tracking error $e_{id}(t) := i_d(t) - i_{d,\text{ref}},\ \forall t \geq 0$, and augment the two integrators for the tracking errors $e_{id}(t)$ and $e_{iq}(t)$ as

$$\dot{z}_{id}(t) = e_{id}(t),\ \dot{z}_{iq}(t) = e_{iq}(t),\ \forall t \geq 0$$

which transforms the error dynamics (9) and (10) into

$$\begin{aligned} c_1\dot{e}_\omega(t) =& -(c_2 + k_{p,\omega}) e_\omega(t) - k_{I,\omega}\tilde{z}_\omega(t) \\ &+ e_{iq}(t) + w_1(t) \qquad (13) \\ \dot{\tilde{z}}_\omega(t) =& e_\omega(t) \qquad (14) \\ \dot{e}_{id}(t) =& -\frac{R_s}{L} e_{id}(t) + \frac{1}{L} u_{d,1}(t) \\ &+ \frac{1}{L}\Big(u_{d,2}(t) + p_1 q_5(t)\Big) \qquad (15) \\ \dot{e}_{iq}(t) =& \frac{1}{L} u_{q,1}(t) + \frac{1}{L}\Big(u_{q,2}(t) + \sum_{i=1}^{4} p_i q_i(t)\Big) \\ &+ w_2(t) \qquad (16) \\ \dot{z}_{id}(t) =& e_{id}(t) \qquad (17) \\ \dot{z}_{iq}(t) =& e_{iq}(t),\ \forall t \geq 0 \qquad (18) \end{aligned}$$

where $u_{d_1}(t)$, $u_{d_2}(t)$, $u_{q,1}(t)$, and $u_{q,2}(t)$ are given by

$$u_d(t) = u_{d,1}(t) + u_{d,2}(t),\ u_q(t) = u_{q,1}(t) + u_{q,2}(t),\ \forall t \geq 0$$

and

$$\tilde{z}_\omega(t) := z_\omega(t) - \frac{p_\omega}{k_{I,\omega}} - \frac{w_{1,0}}{k_{I,\omega}},\ \forall t \geq 0.$$

The unknown coefficients, p_i, $i = 1, \ldots, 4$, are defined by

$$\begin{aligned} p_1 :=& L, \quad p_2 := \frac{3LP\lambda_m k_{P,\omega}}{2J} - R_s \\ p_3 :=& P\lambda_m + \frac{LBk_{P,\omega}}{J}, \quad p_4 := \frac{LT_{L,0}k_{p,\omega}}{J} \end{aligned}$$

$q_i(t)$, $i = 1, \ldots, 5$, denote available signals for feedback given by

$$\begin{aligned} q_1(t) :=& k_{I,\omega} e_\omega(t) - P\omega(t) i_d(t),\ q_2(t) := i_q(t) \\ q_3(t) :=& -\omega(t),\ q_4(t) := -1,\ q_5(t) := P\omega(t) i_q(t)\ \forall t \geq 0 \end{aligned}$$

and $w_2(t)$ refers to the disturbance signal defined by

$$w_2(t) := -\frac{\Delta T_L(t) k_{P,\omega}}{J},\ \forall t \geq 0.$$

The error dynamics, comprised of (13)–(18), can be written in the simple vector form as follows:

$$\begin{aligned} \dot{\mathbf{x}}_\omega(t) =& \mathbf{A}_{\omega,K}\mathbf{x}_\omega(t) + \mathbf{B}_{\omega,1}\mathbf{x}_a(t) + \mathbf{B}_{\omega,d} w_1(t) \qquad (19) \\ \dot{\mathbf{x}}_a(t) =& \mathbf{A}_a \mathbf{x}_a(t) + \mathbf{B}_a \mathbf{u}_1(t) \\ &+ \frac{1}{L}\mathbf{B}_n\Big(\mathbf{u}_2(t) + \mathbf{Q}(t)\mathbf{p}\Big) + \mathbf{B}_d w_2(t) \\ &\forall t \geq 0 \qquad (20) \end{aligned}$$

where the states $\mathbf{x}_\omega(t)$, $\mathbf{x}_a(t)$, and the control inputs $\mathbf{u}_1(t)$, $\mathbf{u}_2(t)$ are given by

$$\mathbf{x}_\omega(t) := \begin{bmatrix} e_\omega(t) \\ \tilde{z}_\omega(t) \end{bmatrix},\ \mathbf{x}_a(t) := \begin{bmatrix} e_{id}(t) \\ e_{iq}(t) \\ z_{id}(t) \\ z_{iq}(t) \end{bmatrix}$$

$$\mathbf{u}_1(t) := \begin{bmatrix} u_{d,1}(t) \\ u_{q,1}(t) \end{bmatrix},\ \mathbf{u}_2(t) := \begin{bmatrix} u_{d,2}(t) \\ u_{q,2}(t) \end{bmatrix},\ \forall t \geq 0.$$

The matrices of the system (19) and (20) are defined as

$$\begin{aligned} \mathbf{A}_{\omega,K} :=& \mathbf{A}_\omega + \mathbf{B}_\omega \mathbf{K}_\omega, \\ \mathbf{A}_\omega :=& \begin{bmatrix} -\frac{c_2}{c_1} & 0 \\ 1 & 0 \end{bmatrix},\ \mathbf{B}_\omega := \begin{bmatrix} \frac{1}{c_1} \\ 0 \end{bmatrix} \\ \mathbf{K}_\omega :=& \begin{bmatrix} -k_{P,\omega} & -k_{I,\omega} \end{bmatrix}, \\ \mathbf{B}_{\omega,1} :=& \begin{bmatrix} 0 & \frac{1}{c_1} & 0 & 0 \\ 0 & 0 & 0 & 0 \end{bmatrix},\ \mathbf{B}_{\omega,d} := \begin{bmatrix} \frac{1}{c_1} \\ 0 \end{bmatrix} \end{aligned}$$

$$\mathbf{A}_a := \begin{bmatrix} -\frac{R_s}{L} & 0 & 0 & 0 \\ 0 & 0 & 0 & 0 \\ 1 & 0 & 0 & 0 \\ 0 & 1 & 0 & 0 \end{bmatrix},\ \mathbf{B}_d := \begin{bmatrix} 0 \\ 1 \\ 0 \\ 0 \end{bmatrix}$$

$$\mathbf{B}_n := \begin{bmatrix} \mathbf{I_{2\times 2}} \\ \mathbf{0}_{2\times 2} \end{bmatrix},\ \mathbf{B}_a := \frac{1}{L}\mathbf{B}_n$$

and the measurable matrix $\mathbf{Q}(t)$ and unknown parameter vector $\mathbf{p}$ are given by

$$\mathbf{Q}(t) := \begin{bmatrix} q_5(t) & 0 & 0 & 0 \\ q_1(t) & q_2(t) & q_3(t) & q_4(t) \end{bmatrix},\ \forall t \geq 0$$

$$\mathbf{p} := \begin{bmatrix} p_1 & p_2 & p_3 & p_4 \end{bmatrix}^T.$$

For stabilizing the system (19) and (20), consider the control law described by

$$\mathbf{u}_1(t) := \mathbf{K}_a \mathbf{x}_a(t) \tag{21}$$

$$\mathbf{u}_2(t) := -\mathbf{Q}(t)\hat{\mathbf{p}}(t),\ \forall t \geq 0 \tag{22}$$

where $\hat{\mathbf{p}}(t)$ is an estimate of the unknown vector $\mathbf{p}$, which is tuned following the adaptation law given by

$$\dot{\hat{\mathbf{p}}} = \Gamma\left(\mathbf{Q}^T(t)\mathbf{B}_n^T\mathbf{P}_a\mathbf{x}_a(t) - \sigma\hat{\mathbf{p}}(t)\right),\ \forall t \geq 0 \tag{23}$$

with $\Gamma = \Gamma^T > \mathbf{0}$, $\mathbf{P}_a = \mathbf{P}_a^T > \mathbf{0}$, $\sigma > 0$ being design parameters. Then, the proposed control law (21) and (22) forces the current error dynamics (20) to be governed by the dynamics

$$\dot{\mathbf{x}}_a(t) = \mathbf{A}_K\mathbf{x}_a(t) + \frac{1}{L}\mathbf{B}_n\mathbf{Q}(t)\tilde{\mathbf{p}}(t) + \mathbf{B}_d w_2(t), \tag{24}$$

$$\dot{\tilde{\mathbf{p}}}(t) = -\Gamma\left(\mathbf{Q}^T(t)\mathbf{B}_n^T\mathbf{P}_a\mathbf{x}_a(t) + \sigma\tilde{\mathbf{p}}(t) - \sigma\mathbf{p}\right),\ \forall t \geq 0 \tag{25}$$

where

$$\mathbf{A}_K := \mathbf{A}_a + \mathbf{B}_a\mathbf{K}_a,\ \tilde{\mathbf{p}}(t) := \mathbf{p} - \hat{\mathbf{p}}(t),\ \forall t \geq 0.$$

Now, we proceed to prove that the proposed control algorithm (21) and (22) globally stabilizes the current error dynamics (24) and (25), which simplifies the proof of the closed-loop stability.

Lemma 1: Define $\mathbf{p}_1 := [R_s \quad L]^T$ and let $\mathbf{p}_{1,i}$, $i = 1, 2, \ldots, 4$, be all possible vectors obtained by substituting the extreme values of the parameters, R_s, L, into the parameter vector $\mathbf{p}_1$, and assume that the four matrix inequalities described by

$$\mathbf{Q}_a\mathbf{A}_{a,i}^T + \mathbf{Y}^T\mathbf{B}_{a,i}^T + \mathbf{A}_{a,i}\mathbf{Q}_a + \mathbf{B}_{a,i}\mathbf{Y} + 2\alpha\mathbf{Q}_a \leq \mathbf{0},\quad i = 1, 2, 3, 4 \tag{26}$$

are solvable for some $\alpha > 0$ and $\mathbf{Q}_a = \mathbf{Q}_a^T > \mathbf{0}$, where

$$(\mathbf{A}_{a,i}, \mathbf{B}_{a,i}) := (\mathbf{A}_a, \mathbf{B}_a)\Big|_{\mathbf{p}_1 = \mathbf{p}_{1,i}},\ i = 1, \ldots, 4.$$

Then, the control gain, defined as

$$\mathbf{K}_a := \mathbf{Y}\mathbf{Q}_a^{-1} \tag{27}$$

with setting $\mathbf{P}_a = \mathbf{Q}_a^{-1}$ for the adaptation law (23), globally stabilizes the current error dynamics (24) and (25) for any $\Gamma = \Gamma^T > \mathbf{0}$, $\sigma > 0$.

Proof: Consider the positive definite function defined as

$$V(\mathbf{x}_a(t), \tilde{\mathbf{p}}(t)) := \mathbf{x}_a^T(t)\mathbf{P}_a\mathbf{x}_a(t) + \frac{1}{L}\tilde{\mathbf{p}}^T(t)\Gamma^{-1}\tilde{\mathbf{p}}(t),\ \forall t \geq 0 \tag{28}$$

where $\mathbf{Q}_a = \mathbf{P}_a^{-1}$ solves the four inequalities in (26). Its time derivative along the trajectory of the closed-loop current error dynamics (24) and (25) is given by

$$\begin{aligned} \dot{V} =\ & \dot{\mathbf{x}}_a^T(t)\mathbf{P}_a\mathbf{x}_a(t) + \mathbf{x}_a^T(t)\mathbf{P}_a\dot{\mathbf{x}}_a(t) + \frac{2}{L}\tilde{\mathbf{p}}^T(t)\Gamma^{-1}\dot{\tilde{\mathbf{p}}}(t) \\ =\ & \left(\mathbf{A}_K\mathbf{x}_a(t) + \frac{1}{L}\mathbf{B}_n\mathbf{Q}(t)\tilde{\mathbf{p}}(t) + \mathbf{B}_d w_2(t)\right)^T\mathbf{P}_a\mathbf{x}_a(t) \\ & + \mathbf{x}_a^T(t)\mathbf{P}_a\left(\mathbf{A}_K\mathbf{x}_a(t) + \frac{1}{L}\mathbf{B}_n\mathbf{Q}(t)\tilde{\mathbf{p}}(t) + \mathbf{B}_d w_2(t)\right) \\ & - \frac{2}{L}\tilde{\mathbf{p}}^T(t)\left(\mathbf{Q}^T(t)\mathbf{B}_n^T\mathbf{P}_a\mathbf{x}_a(t) + \sigma\tilde{\mathbf{p}}(t) - \sigma\mathbf{p}\right) \\ =\ & \mathbf{x}_a^T(t)\left(\mathbf{A}_K^T\mathbf{P}_a + \mathbf{P}_a\mathbf{A}_K\right)\mathbf{x}_a(t) \\ & + \frac{2}{L}\tilde{\mathbf{p}}^T(t)\mathbf{Q}^T(t)\mathbf{B}_n^T\mathbf{P}_a\mathbf{x}_a(t) + 2\mathbf{x}_a^T(t)\mathbf{P}_a\mathbf{B}_d w_2(t) \\ & - \frac{2}{L}\tilde{\mathbf{p}}^T(t)\mathbf{Q}^T(t)\mathbf{B}_n^T\mathbf{P}_a\mathbf{x}_a(t) \\ & - \frac{2\sigma}{L}\|\tilde{\mathbf{p}}(t)\|^2 + \frac{2\sigma}{L}\tilde{\mathbf{p}}^T(t)\mathbf{p},\ \forall t \geq 0. \end{aligned}$$

Because the four linear matrix inequality (LMI) (26) result in four inequalities

$$\left(\mathbf{A}_K^T\mathbf{P}_a + \mathbf{P}_a\mathbf{A}_K\right)\Big|_{\mathbf{p}_1 = \mathbf{p}_{1,i}} = (\mathbf{A}_{a,1} + \mathbf{B}_{a,1}\mathbf{K}_a)^T\mathbf{P}_a + \mathbf{P}_a(\mathbf{A}_{a,1} + \mathbf{B}_{a,1}\mathbf{K}_a) \leq -2\alpha\mathbf{P}_a \quad i = 1, 2, 3, 4$$

respectively, it holds that

$$\mathbf{A}_K^T\mathbf{P}_a + \mathbf{P}_a\mathbf{A}_K \leq -2\alpha\mathbf{P}_a$$

for any R_s, L satisfying (5) based on the result in [28]. Thus, it follows that:

$$\begin{aligned} \dot{V} \leq\ & -2\alpha\mathbf{x}_a^T(t)\mathbf{P}_a\mathbf{x}_a(t) - \frac{2\sigma}{L}\|\tilde{\mathbf{p}}(t)\|^2 \\ & + 2\mathbf{x}_a^T(t)\mathbf{P}_a\mathbf{B}_d w_2(t) + \frac{2\sigma}{L}\tilde{\mathbf{p}}^T(t)\mathbf{p},\ \forall t \geq 0. \end{aligned}$$

Since the two indefinite terms satisfy that

$$\frac{2\sigma}{L}\tilde{\mathbf{p}}^T(t)\mathbf{p} \le \frac{\sigma}{L}\|\tilde{\mathbf{p}}(t)\|^2 + \frac{\sigma}{L}\|\mathbf{p}\|^2,\ \forall t, \tag{29}$$

$$\begin{aligned} 2\mathbf{x}_a^T(t)\mathbf{P}_a\mathbf{B}_d w_2(t) &\le \alpha\mathbf{x}_a^T(t)\mathbf{P}_a\mathbf{x}_a(t) + \frac{1}{\alpha}\|\mathbf{P}_a^{1/2}\mathbf{B}_d w_2(t)\|^2 \\ &\le \alpha\mathbf{x}_a^T(t)\mathbf{P}_a\mathbf{x}_a(t) + \frac{1}{\alpha}\|\mathbf{P}_a^{1/2}\mathbf{B}_d\|^2\bar{w}_2^2 \\ &\quad \forall t \ge 0 \end{aligned} \tag{30}$$

by utilizing Young's inequality, i.e.,

$$2\mathbf{x}^T\mathbf{y} \le \epsilon\|\mathbf{x}\|^2 + \frac{1}{\epsilon}\|\mathbf{y}\|^2,\ \forall \mathbf{x},\mathbf{y} \in \mathbb{R}^n,\ \forall \epsilon > 0$$

and the inequality

$$|w_2(t)| \le \bar{w}_2 := \frac{\beta|k_{p,\omega}|}{J},\ \forall t \ge 0$$

where $\beta > 0$ is a bound of $\Delta T_L(t)$ defined in (6). The two inequalities (29) and (30) yield that

$$\begin{aligned} \dot{V} &\le -\alpha\mathbf{x}_a^T(t)\mathbf{P}_a\mathbf{x}_a(t) - \frac{\sigma}{L}\|\tilde{\mathbf{p}}(t)\|^2 + r - \alpha\mathbf{x}_a^T(t)\mathbf{P}_a\mathbf{x}_a(t) \\ &\quad - \frac{\sigma}{4\lambda_{\max}(\Gamma^{-1})}\frac{4}{L}\lambda_{\max}(\Gamma^{-1})\|\tilde{\mathbf{p}}(t)\|^2 + r \\ &\le -\alpha\mathbf{x}_a^T(t)\mathbf{P}_a\mathbf{x}_a(t) - \frac{\sigma}{4\lambda_{\max}(\Gamma^{-1})}\frac{4}{L}\tilde{\mathbf{p}}^T(t)\Gamma^{-1}\tilde{\mathbf{p}}(t) + r \\ &\le -\gamma V + r,\ \forall t \ge 0 \end{aligned} \tag{31}$$

which implies the global stability of the closed-loop current error dynamics (24), (25), where the positive constants γ and r are defined as

$$\begin{aligned} \gamma &:= \min\left\{\alpha, \frac{\sigma}{4\lambda_{\max}(\Gamma^{-1})}\right\}, \\ r &:= \frac{\sigma}{L}\|\mathbf{p}\|^2 + \frac{1}{\alpha}\|\mathbf{P}_a^{1/2}\mathbf{B}_d\|^2\bar{w}_2^2 \end{aligned} \tag{32}$$

and the second inequality comes from the following relationship:

$$\begin{aligned} \lambda_{\min}(\mathbf{A})\|\mathbf{x}\|^2 \le\ & \mathbf{x}^T\mathbf{A}\mathbf{x} \le \lambda_{\max}(\mathbf{A})\|\mathbf{x}\|^2 \\ \forall \mathbf{x} \in \mathbb{R}^n,\quad & \forall\ \mathbf{A} = \mathbf{A}^T > \mathbf{0} \end{aligned}$$

with $\lambda_{\min}((\cdot))$ and $\lambda_{\max}((\cdot))$ being the minimum and maximum eigenvalues of the matrix $(\cdot)$, respectively. ■

Remark 1: The controllability of the pair $(\mathbf{A}_a, \mathbf{B}_a)$ is a necessary condition to guarantee the existence of a solution to the four inequalities in (26), which can be verified by checking whether its controllability matrix $\mathcal{C} := [\,\mathbf{B_a}\ \mathbf{A}_a\mathbf{B}_a\,] (\in \mathbb{R}^{4\times 4})$ has full rank or not. For instance,

$$\begin{aligned} \text{rank}(\mathcal{C}) &= \text{rank}\left(\left[\,\mathbf{B_a}\ \mathbf{A}_a\mathbf{B}_a\,\right]\right) \\ &= \text{rank}\left(\begin{bmatrix} \frac{1}{L}\mathbf{I}_{2\times 2} & * \\ \mathbf{0}_{2\times 2} & \frac{1}{L}\mathbf{I}_{2\times 2} \end{bmatrix}\right) = 4, \\ &\quad \forall R_s > 0,\ \forall L > 0 \end{aligned}$$

which indicates the controllability of the pair $(\mathbf{A}_a, \mathbf{B}_a)$.

Remark 2: Assuming $\tilde{\mathbf{p}}(t) = \mathbf{0},\ \forall t$, and defining

$$V_{\text{nom}}(\mathbf{x}_a(t)) := V(\mathbf{x}_a(t), \tilde{\mathbf{p}}(t))\Big|_{\tilde{\mathbf{p}}(t)=0},\ \forall t \ge 0$$

it follows from the inequality in (31) that:

$$\begin{aligned} \dot{V}_{\text{nom}} &\le -\frac{\alpha}{2}V_{\text{nom}} - \frac{\alpha}{2}\mathbf{x}_a^T(t)\mathbf{P}_a\mathbf{x}_a(t) + r \\ &\le -\frac{\alpha}{2}V_{\text{nom}} \\ &\quad -\left(\frac{\alpha}{2}\lambda_{\min}(\mathbf{P}_a) - \frac{r}{\|\mathbf{x}_a(t)\|^2}\right)\|\mathbf{x}_a(t)\|^2 \\ &\le -\frac{\alpha}{2}V_{\text{nom}}, \\ &\quad \forall\|\mathbf{x}_a(t)\| \ge \sqrt{\frac{2r}{\alpha\lambda_{\min}(\mathbf{P}_a)}},\ \forall t \ge 0 \end{aligned}$$

which implies that

$$\begin{aligned} \|\mathbf{x}_a(t)\| &\le e^{-\frac{\alpha}{4}t}\kappa(\mathbf{P}_a)\|\mathbf{x}_a(0)\|, \\ \forall\|\mathbf{x}_a(t)\| &\ge \sqrt{\frac{2r}{\alpha\lambda_{\min}(\mathbf{P}_a)}},\ \forall t \ge 0 \end{aligned} \tag{33}$$

(for details, see Comparison Principle in [29]), where

$$\kappa(\mathbf{P}_a) := \sqrt{\frac{\lambda_{\max}(\mathbf{P}_a)}{\lambda_{\min}(\mathbf{P}_a)}}.$$

The inequality in (33) dictates that, to maximize the decay ratio of the current tracking error $\mathbf{x}_a(t)$, it is desirable to determine the control gain of (27) by solving the optimization problem described by

$$\max_{\alpha>0, \mathbf{Q}_a=\mathbf{Q}_a^T>\mathbf{0}, \mathbf{Y}} \alpha \quad \text{subject to (26)} \tag{34}$$

which can be easily solved using semidefinite programming such as YALMIP and FMINCON of the MATLAB software. The optimization problem described in (34) can be also used as the current-loop control gain selection guideline. This result is in contrast to the result in [21].

Remark 3: Thanks to the introduced integral action of (17) and (18) with vector representations of (19) and (20), it is possible to guarantee the offset-free property that is given by

$$e_{id,\infty} = 0, e_{iq,\infty} = 0$$

where $e_{id,\infty}$ and $e_{iq,\infty}$ denote the steady-state values of $e_{id}(t)$ and $e_{iq}(t)$, respectively, which is another contrast to the previous result of [21].

Note that, since Lemma 1 asserts only that the proposed control law (21), (22) stabilizes the current tracking error dynamics (20) for a subsystem of the closed-loop system (19), (20), it is unknown whether the control law (21), (22) also stabilizes the closed-loop system including the dynamics (19). Theorem 1 presents a method for assigning a robust stabilizing control gain for the closed-loop system (19), (20), (21), and (22) using the result of Lemma 1.

Theorem 1: Define $\mathbf{p}_2 := [\,J \quad \lambda_m \quad B\,]^T$ and let $\mathbf{p}_{2,i}$, $i = 1, 2, \ldots, 8$, be all possible vectors obtained by substituting the

extreme values of the parameters, J, λ_m, and B, into the parameter vector $\mathbf{p}_2$. Suppose that the assumption of Lemma 1 holds so that it is acceptable to pick the stabilizing current-loop control gain in the form of (27), and that there exists $\mathbf{Q}_\omega = \mathbf{Q}_\omega^T > \mathbf{0}$ such that it solves the inequalities

$$\left[\begin{array}{cc} \mathbf{F}(\mathbf{Q}_\omega, \mathbf{Y}_\omega, \beta) & \mathbf{B}_{\omega,1} \\ \mathbf{B}_{\omega,1}^T & -(\alpha-\beta)\mathbf{P}_a \end{array}\right]\Big|_{\mathbf{p}=\mathbf{p}_{2,i}} \leq \mathbf{0},\ i = 1, 2, \ldots, 8 \tag{35}$$

for some $\beta \in (0, \alpha)$, where

$$\begin{aligned}\mathbf{F}(\mathbf{Q}_\omega, \mathbf{Y}_\omega, \beta) :\ =\ & \mathbf{Q}_\omega \mathbf{A}_\omega^T + \mathbf{Y}_\omega^T \mathbf{B}_\omega + \mathbf{A}_\omega \mathbf{Q}_\omega \\ & + \mathbf{B}_\omega \mathbf{Y}_\omega + \beta \mathbf{Q}_\omega\end{aligned}$$

and the pair $(\alpha, \mathbf{P}_a)$ is a solution to the four inequalities in (26). Then, the speed control gain, which is determined by

$$\mathbf{K}_\omega = \mathbf{Y}_\omega \mathbf{Q}_\omega^{-1} \tag{36}$$

with the current control gain of (27) and the setting $\mathbf{P}_a = \mathbf{Q}_a^{-1}$ for the adaptation law (23), globally stabilizes the closed-loop system comprised of (19), (20), (21), and (22) for all $\Gamma = \Gamma^T > \mathbf{0}$, $\sigma > 0$.

Proof: Define

$$\mathbf{x}_{cl}(t) := \left[\begin{array}{c} \mathbf{x}_\omega(\mathbf{t}) \\ \mathbf{x}_a(t) \end{array}\right],\ \forall t \geq 0,\ \mathbf{P}_{cl} := \left[\begin{array}{cc} \mathbf{P}_\omega & \mathbf{0}_{2\times 4} \\ \mathbf{0}_{4\times 2} & \mathbf{P}_a \end{array}\right]$$

and consider the composite positive definite function defined by

$$\begin{aligned} V_{cl}(\mathbf{x}_{cl}(t), \tilde{\mathbf{p}}(t)) :=\ & \mathbf{x}_{cl}^T(t)\mathbf{P}_{cl}\mathbf{x}_{cl}(t) + \frac{1}{L}\tilde{\mathbf{p}}^T(t)\Gamma^{-1}\tilde{\mathbf{p}}(t) \\ =\ & \mathbf{x}_\omega^T(t)\mathbf{P}_\omega\mathbf{x}_\omega(t) + V(\mathbf{x}_a(t), \tilde{\mathbf{p}}(t)),\ \forall t \geq 0 \end{aligned}$$

where the positive definite function $V(\mathbf{x}_a(t), \tilde{\mathbf{p}}(t))$ is defined in (28). Then, its time derivative along the closed-loop trajectory of the system (19), (20), (21), (22), and (23) is given by

$$\begin{aligned} \dot{V}_{cl} =\ & \Big[\mathbf{A}_{\omega,K}\mathbf{x}_\omega(t) + \mathbf{B}_{\omega,1}\mathbf{x}_a(t) + \mathbf{B}_{\omega,d}w_1(t)\Big]^T \mathbf{P}_\omega\mathbf{x}_\omega(t) \\ & + \mathbf{x}_\omega^T(t)\mathbf{P}_\omega\Big[\mathbf{A}_{\omega,K}\mathbf{x}_\omega(t) + \mathbf{B}_{\omega,1}\mathbf{x}_a(t) + \mathbf{B}_{\omega,d}w_1(t)\Big] \\ & + \dot{V} \\ \leq\ & \mathbf{x}_\omega^T(t)\Big(\mathbf{A}_{\omega,K}^T\mathbf{P}_\omega + \mathbf{P}_\omega\mathbf{A}_{\omega,K}\Big)\mathbf{x}_\omega(t) \\ & + 2\mathbf{x}_\omega^T(t)\mathbf{P}_\omega\mathbf{B}_{\omega,1}\mathbf{x}_a(t) + 2\mathbf{x}_\omega^T(t)\mathbf{P}_\omega\mathbf{B}_{\omega,d}w_1(t) \\ & - \alpha\mathbf{x}_a^T(t)\mathbf{P}_a\mathbf{x}_a(t) - \frac{\sigma}{L}\|\tilde{\mathbf{p}}(t)\|^2 + r \\ =\ & \mathbf{x}_{cl}^T(t)\left[\begin{array}{cc} \mathbf{A}_{\omega,\mathbf{K}}^{\mathbf{T}}\mathbf{P}_\omega + \mathbf{P}_\omega\mathbf{A}_{\omega,\mathbf{K}} & \mathbf{P}_\omega\mathbf{B}_{\omega,1} \\ \mathbf{B}_{\omega,1}^T\mathbf{P}_\omega & -\alpha\mathbf{P}_a \end{array}\right]\mathbf{x}_{cl}(t) \\ & - \frac{\sigma}{L}\|\tilde{\mathbf{p}}(t)\|^2 + 2\mathbf{x}_\omega^T(t)\mathbf{P}_\omega\mathbf{B}_{\omega,d}w_1(t) + r \\ \leq\ & -\beta\mathbf{x}_{cl}^T(t)\mathbf{P}_{cl}\mathbf{x}_{cl}(t) - \frac{\sigma}{L}\|\tilde{\mathbf{p}}(t)\|^2 \\ & + 2\mathbf{x}_\omega^T(t)\mathbf{P}_\omega\mathbf{B}_{\omega,d}w_1(t) + r,\ \forall t \geq 0 \end{aligned} \tag{37}$$

for all parameters, J, λ_m, and B, satisfying (5), where the first inequality is obtained using the inequality (31) of Lemma 1. Note that, because the eight inequalities in (35) yield that

$$\begin{aligned} & \left[\begin{array}{cc} \mathbf{A}_{\omega,\mathbf{K}}^{\mathbf{T}}\mathbf{P}_\omega + \mathbf{P}_\omega\mathbf{A}_{\omega,\mathbf{K}} & \mathbf{P}_\omega\mathbf{B}_{\omega,1} \\ \mathbf{B}_{\omega,1}^T\mathbf{P}_\omega & -\alpha\mathbf{P}_a \end{array}\right]\Big|_{\mathbf{p}=\mathbf{p}_{2,i}} \\ & \leq -\beta\left[\begin{array}{cc} \mathbf{P}_\omega & \mathbf{0}_{2\times 4} \\ \mathbf{0}_{4\times 2} & \mathbf{P}_a \end{array}\right] = -\beta\mathbf{P}_{cl},\ i = 1, \ldots, 8 \end{aligned}$$

the last inequality in (37) is satisfied due to the result of [28]. Furthermore, applying Young's inequality to the indefinite term of (37), we find that

$$\begin{aligned} & 2\mathbf{x}_\omega^T(t)\mathbf{P}_\omega\mathbf{B}_{\omega,d}w_1(t) \\ & \leq \frac{\beta}{2}\mathbf{x}_\omega^T(t)\mathbf{P}_\omega\mathbf{x}_w(t) + \frac{2}{\beta}\|\mathbf{P}_\omega^{1/2}\mathbf{B}_{\omega,d}\|^2\bar{w}_1^2 \\ & \leq \frac{\beta}{2}\mathbf{x}_\omega^T(t)\mathbf{P}_\omega\mathbf{x}_w(t) + \frac{\beta}{2}\mathbf{x}_a^T(t)\mathbf{P}_a\mathbf{x}_a(t) + \frac{2}{\beta}\|\mathbf{P}_\omega^{1/2}\mathbf{B}_{\omega,d}\|^2\bar{w}_1^2 \\ & = \frac{\beta}{2}\mathbf{x}_{cl}^T(t)\mathbf{P}_{cl}\mathbf{x}_{cl}(t) + \frac{2}{\beta}\|\mathbf{P}_\omega^{1/2}\mathbf{B}_{\omega,d}\|^2\bar{w}_1^2,\ \forall t \geq 0 \end{aligned}$$

which implies that

$$\begin{aligned} \dot{V}_{cl} \leq\ & -\frac{\beta}{2}\mathbf{x}_{cl}^T(t)\mathbf{P}_{cl}\mathbf{x}_{cl}(t) - \frac{\sigma}{L}\|\tilde{\mathbf{p}}(t)\|^2 + r_{cl} \\ =\ & -\frac{\beta}{2}\mathbf{x}_{cl}^T(t)\mathbf{P}_{cl}\mathbf{x}_{cl}(t) \\ & -\frac{\sigma}{4\lambda_{\max}(\Gamma^{-1})}\frac{4}{L}\lambda_{\max}(\Gamma^{-1})\|\tilde{\mathbf{p}}(t)\|^2 + r_{cl} \\ \leq\ & -\gamma_{cl}V_{cl} + r_{cl},\ \forall t \geq 0 \end{aligned} \tag{38}$$

where

$$\gamma_{cl} := \min\left\{\frac{\beta}{2},\ \frac{\sigma}{4\lambda_{\max}(\Gamma^{-1})}\right\},\ r_{cl} := r + \frac{2}{\beta}\|\mathbf{P}_\omega^{1/2}\mathbf{B}_{\omega,d}\|^2\bar{w}_1^2.$$

Therefore, the closed-loop system is globally stable. ■

Remark 4: Assuming $\tilde{\mathbf{p}}(t) = \mathbf{0},\ \forall t$, and defining

$$V_{cl,\text{nom}}(\mathbf{x}_{cl}(t)) := V_{cl}(\mathbf{x}_{cl}(t), \tilde{\mathbf{p}}(t))\Big|_{\tilde{\mathbf{p}}(t)=0},\ \forall t \geq 0,$$

it follows from the inequality in (38) that:

$$\begin{aligned} \dot{V}_{cl,\text{nom}} \leq\ & -\frac{\beta}{4}V_{cl,\text{nom}} - \frac{\beta}{4}\mathbf{x}_{cl}^T(t)\mathbf{P}_{cl}\mathbf{x}_{cl}(t) + r_{cl} \\ \leq\ & -\frac{\beta}{4}V_{cl,\text{nom}} \\ & -\left(\frac{\beta}{4}\lambda_{\min}(\mathbf{P}_{cl}) - \frac{r_{cl}}{\|\mathbf{x}_{cl}(t)\|^2}\right)\|\mathbf{x}_{cl}(t)\|^2 \\ \leq\ & -\frac{\beta}{4}V_{cl,\text{nom}}, \\ & \forall\|\mathbf{x}_{cl}(t)\| \geq \sqrt{\frac{4r_{cl}}{\beta\lambda_{\min}(\mathbf{P}_{cl})}},\ \forall t \geq 0 \end{aligned}$$

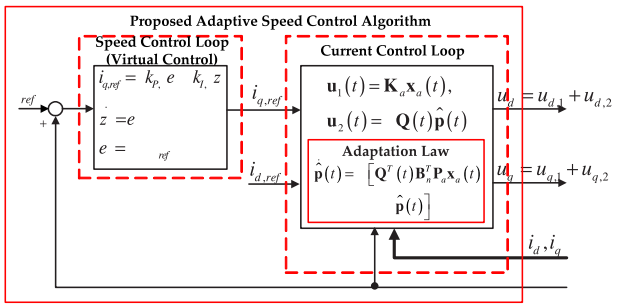

Fig. 1. Structure of the proposed control law.

which leads to

$$\|\mathbf{x}_{cl}(t)\| \le e^{-\frac{\beta}{8}t}\kappa(\mathbf{P}_{cl})\|\mathbf{x}_{cl}(0)\|,$$
$$\forall\|\mathbf{x}_{cl}(t)\| \ge \sqrt{\frac{4r_{cl}}{\beta\lambda_{\min}(\mathbf{P}_{cl})}},\ \forall t \ge 0 \tag{39}$$

(for details, see Comparison Principle in [29]), where

$$\kappa(\mathbf{P}_{cl}) := \sqrt{\frac{\lambda_{\max}(\mathbf{P}_{cl})}{\lambda_{\min}(\mathbf{P}_{cl})}}.$$

The inequality in (39) indicates that, to maximize the decay ratio of the tracking error $\mathbf{x}_{cl}(t)$, it is desirable to determine the control gain of (36) by solving the optimization problem described by

$$\max_{\beta>0,\mathbf{Q}_\omega=\mathbf{Q}_\omega^T>\mathbf{0},\mathbf{Y}_\omega} \beta \quad \text{subject to (35)} \tag{40}$$

which can be easily solved using semidefinite programming such as YALMIP and FMINCON of the MATLAB software. The optimization problem of (40) can be also used as the speed-loop control gain selection guideline. This is in contrast to the result in [21].

Remark 5: The controllability of the pair $(\mathbf{A}_\omega, \mathbf{B}_\omega)$ is a necessary condition to guarantee the existence of a solution to the eight inequalities in (35), which can be verified by checking whether its controllability matrix $\mathcal{C}_\omega := [\mathbf{B}_\omega \ \mathbf{A}_\omega\mathbf{B}_\omega] (\in \mathbb{R}^{2\times 2})$ has a full rank or not. In particular,

$$\text{rank}\,(\mathcal{C}_\omega) = \text{rank}\left(\begin{bmatrix}\mathbf{B}_\omega & \mathbf{A}_\omega\mathbf{B}_\omega\end{bmatrix}\right)$$
$$= \text{rank}\left(\frac{1}{c_1}\begin{bmatrix}1 & -\frac{c_2}{c_1}\\ 0 & 1\end{bmatrix}\right) = 2,\ \forall J, \lambda_m, B > 0$$

which leads the controllability of the pair $(\mathbf{A}_\omega, \mathbf{B}_\omega)$.

Remark 6: The integral action introduced in the virtual control input (12) guarantees that the steady-state errors of the speed tracking error $e_\omega(t)$ are zero in the actual implementation, which is another contrast to [21].

Remark 7: The proposed control law presented in (11) and (12) can be decomposed into two parts: the speed-control loop and the current-control loop, which is shown in Fig. 1.

In this figure, the virtual control signal $i_{q,\text{ref}}(t)$ used in (8) can be interpreted as the q-frame current reference signal of the classical cascade PI controller. Thus, it is easy to see that the q-frame current can be limited by constraining its reference signal $i_{q,\text{ref}}(t)$ by applying the antiwindup method used in the classical cascade PI method.

Remark 8: For the proposed control law (21), (22), (23), the control gain selection guideline is recapitulated as follows:

1) solve the optimization problem (34) using semidefinite programming with respect to variables α, $\mathbf{Q}_a$, and $\mathbf{Y}$;
2) using the solution $(\alpha^*, \mathbf{Q}_a^*, \mathbf{Y}^*)$ obtained in Step 1, calculate the stabilizing current-control gain as

$$\mathbf{K}_a^* = \mathbf{Y}^*(\mathbf{Q}_a^*)^{-1};$$

3) using the solution $(\alpha^*, \mathbf{Q}_a^*, \mathbf{Y}^*)$ obtained in Step 1, solve the optimization problem in (40) using semidefinite programming with respect to variables β, $\mathbf{Q}_\omega$, and $\mathbf{Y}_\omega$;
4) using the solution $(\beta^*, \mathbf{Q}_\omega^*, \mathbf{Y}_\omega^*)$ obtained in Step 3, calculate the stabilizing speed control gain as

$$\mathbf{K}_\omega^* = \mathbf{Y}_\omega^*(\mathbf{Q}_\omega^*)^{-1};$$

5) setting $\mathbf{P}_a = (\mathbf{Q}_a^*)^{-1}$ for the adaptation law (23), tune the adaptation gain $\Gamma = \Gamma^T > \mathbf{0}$ until a satisfactory transient response is achieved (trial-and-error method).

IV. Simulations

This section carries out the simulations using the PSIM software in order to show the closed-loop robustness of the proposed method against the parameter variations, comparing it to the classical cascade PI method, which includes a F/F compensation term. It was assumed that the true parameters of SPMSM are given by

$$R_s = 2.2\ \Omega,\ L = 3.05\ \text{mH},\ \lambda_m = 0.477\ \text{Wb},\ P = 12,$$
$$J = 0.2\ \text{kgm}^2,\ B = 10\ \text{Nm/rad/s}, \tag{41}$$

and a dc-source voltage V_{dc} at 450 V was chosen for operating the three-phase inverter. The sampling and space vector pulse-width modulation (SVPWM) periods were set to be 0.1 ms, respectively. The configurations of the two closed-loop systems are described in Fig. 2.

The lower and upper bounds of the SPMSM parameters were chosen as follows:

$$R_{s,\min} = 1.1\ \Omega(=0.5R_s),\ R_{s,\max} = 4.4\ \Omega(=2R_s),$$
$$L_{\min} = 1.5\ \text{mH}(=0.5L),\ L_{\max} = 6.1\ \text{mH}(=2L),$$
$$\lambda_{m,\min} = 0.2385\ Wb(=0.5\,\lambda_m),$$
$$\lambda_{m,\max} = 0.954\ Wb(=2\,\lambda_m),$$
$$J_{\min} = 0.1\ \text{kgm}^2(=0.5J),\ J_{\max} = 0.4\ \text{kgm}^2(=2J),$$
$$B_{\min} = 5\ \text{Nm/rad/s}(=0.5B),$$
$$B_{\max} = 20\ \text{Nm/rad/s}(=2B),$$

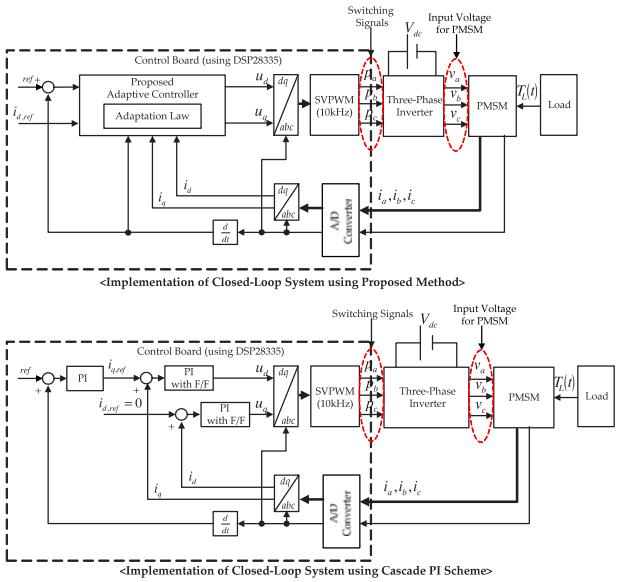

Fig. 2. Configuration of the implemented closed-loop system.

which yields the control gains of the current loop and speed loop using the guideline described in Remark 8 as

$$\mathbf{K}_a = \begin{bmatrix} -11.07 & 0 & -12536 & 0 \\ 0 & -9.94 & 0 & -7855 \end{bmatrix}$$
$$\mathbf{K}_\omega = \begin{bmatrix} -4.2 & -124.6 \end{bmatrix},$$
$$\Gamma = \text{diag}\Big\{0.0001, 0.01, 0.01, 0.01\Big\},\ \sigma = 1 \times 10^{-10}$$

with $\alpha = 300$, $\beta = 4$

$$\mathbf{P}_a = \begin{bmatrix} 0.0004 & 0 & 0.3325 & 0 \\ 0 & 0.0006 & 0 & 0.4722 \\ 0.3325 & 0 & 533.4 & 0 \\ 0 & 0.4722 & 0 & 661.1 \end{bmatrix}$$
$$\mathbf{P}_\omega = 10^{-4} \times \begin{bmatrix} 1 & 1.2 \\ 1.2 & 363 \end{bmatrix},$$
$$\mathbf{Q}_a = \begin{bmatrix} 5200 & 0 & -3.2 & 0 \\ 0 & 3806 & 0 & -2.7 \\ -3.2 & 0 & 0.004 & 0 \\ 0 & -2.7 & 0 & 0.004 \end{bmatrix}$$
$$\mathbf{Q}_\omega = 10^4 \times \begin{bmatrix} 5.7 & -0.18 \\ -0.18 & 0.009 \end{bmatrix}$$
$$\mathbf{Y} = \begin{bmatrix} -16900 & 0 & -10 & 0 \\ 0 & -16500 & 0 & -0.1113 \end{bmatrix}$$
$$\mathbf{Y}_\omega = 10^4 \times \begin{bmatrix} -1.18 & -0.31 \end{bmatrix}.$$

The cascade PI speed-control scheme with the F/F compensation term used for a comparison is described by

$$u_d(t) = -k_{P,id} e_{id}(t) - k_{I,id} \int_0^t e_{id}(\tau) d\tau - P\omega(t) L_0 i_q(t), \quad (42)$$
$$u_q(t) = -k_{P,iq} e_{iq}(t) - k_{I,iq} \int_0^t e_{iq}(\tau) d\tau + P\omega(t)\Big(L_0 i_d(t) + \lambda_{m,0}\Big),\ \forall t \geq 0 \quad (43)$$

where $e_{id}(t) = i_d(t) - i_{d,ref}$, $e_{iq}(t) = i_q(t) - i_{q,\text{ref}}$, $\forall t \geq 0$, and the q-frame current reference signal $i_{q,\text{ref}}(t)$ is given by

$$i_{q,\text{ref}}(t) = -k_{P,\omega} e_\omega(t) - k_{I,\omega} \int_0^t e_\omega(\tau) d\tau,\ \forall t \geq 0. \quad (44)$$

$L_0 \in [L_{\min}, L_{\max}]$ and $\lambda_{m,0} \in [\lambda_{m,\min}, \lambda_{m,\max}]$ denote the nominal values of L and λ_m, respectively. For the selection of PI gain values, we assumed that the nominal parameter values of the SPMSM are

$$R_{s,0} = 3.3\ \Omega\ (= 1.5 R_s),\ L_0 = 1.5\ \text{mH}\ (= 0.5\ L)$$
$$\lambda_{m,0} = 0.7155\ \text{Wb}(= 1.5\lambda_m)$$
$$B_0 = 15\ \text{Nm/rad/s}\ (= 1.5B)$$
$$J_0 = 0.1\ \text{kgm}^2 (= J_{\min}) \quad (45)$$

which yields the inner-loop PI gains of

$$k_{P,id} = L_0\omega_c,\ k_{I,id} = R_{s,0}\omega_c$$
$$k_{P,iq} = L_0\omega_c,\ k_{I,iq} = R_{s,0}\omega_c \quad (46)$$

where ω_c stands for the cutoff frequency, which can be used as a design parameter. The F/F compensation terms were also constructed using the nominal SPMSM parameters in (45). In this experimental study, the cutoff frequency ω_c was set to 1 kHz. Note that it is easily verified that the PI gains of (46) constitute the closed-loop transfer function $G(s)$ from $i_{d,\text{ref}}$ $(i_{q,\text{ref}})$ to i_d (i_q) to be

$$G(s) = \frac{\omega_c}{s + \omega_c}$$

provided that the nominal SPMSM parameters of (45) are the same as the true values of (41), where s refers to the complex variable. The outer-loop speed PI gains were chosen as

$$k_{P,\omega} = \frac{2J_0}{3P\lambda_{m,0}}\left(\omega_{\text{cs}} - \frac{B_0}{J_0}\right),\ k_{I,\omega} = \frac{2J_0\omega_{\text{cs}}^2}{15P\lambda_{m,0}}$$

so that the closed-loop transfer function $G_\omega(s)$ from the input ω_{ref} to the output ω given by

$$G_\omega(s) = \frac{\omega_n^2}{s^2 + 2\zeta\omega_n s + \omega_n^2}$$

holds as long as the nominal parameter values exactly equal to their true values where ω_{cs} denotes the bandwidth of the outer-loop PI controller as the tuning parameter, and the two constants

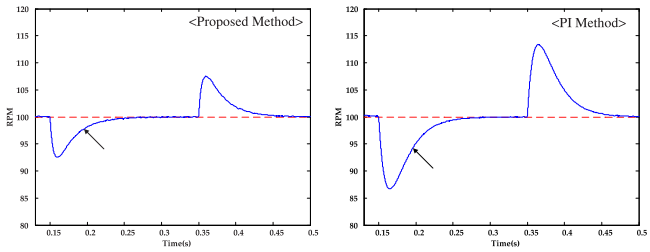

Fig. 3. SPMSM speed regulation performance comparison between the proposed method and the PI method at the 100 r/min operation for a load torque change.

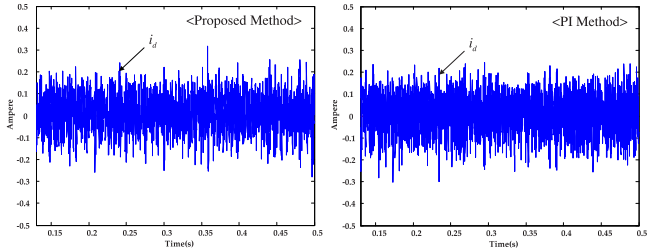

Fig. 4. d-frame current behavior comparison between the proposed method and the PI method at 100 r/min operation for a load torque change.

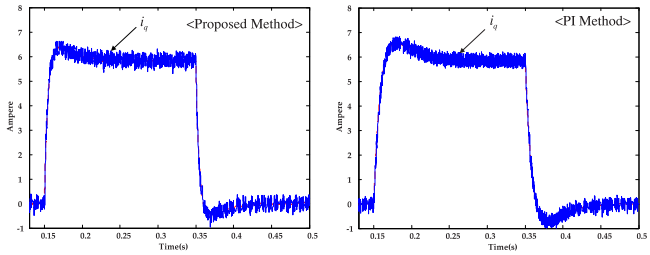

Fig. 5. q-frame current behavior comparison between the proposed method and the PI method at 100 r/min operation for a load torque change.

ζ, ω_n are defined as

$$\zeta := \frac{\sqrt{5}}{2}, \quad \omega_n = \frac{\omega_{\rm cs}}{\sqrt{5}}.$$

The bandwidth parameter $\omega_{\rm cs}$ was tuned as $\omega_{\rm cs} = 250$ Hz for the best convergence rate with a tolerable overshoot.

The simulations were performed to compare the speed regulation performances at the 100 r/min operation in regard to the load torque variations where the load torque 50 Nm is applied and, then, removed in a sequential manner.

In the first simulation, the parameters of the SPMSM block in the PSIM software were chosen to be the same as the true parameters described in (41). The resulting speed and current responses are presented in Figs. 3–6, which shows that there is no significant difference between the proposed method and the PI method.

In the second simulation, the inductance value of the SPMSM block in the PSIM software was changed from $L = 3.05$ mH to $L = 1.05$ mH $(= L_{\rm min})$, and the rest of the SPMSM parameters were left the same as the first simulation. Figs. 7–10 present the corresponding speed and current responses, which turns out

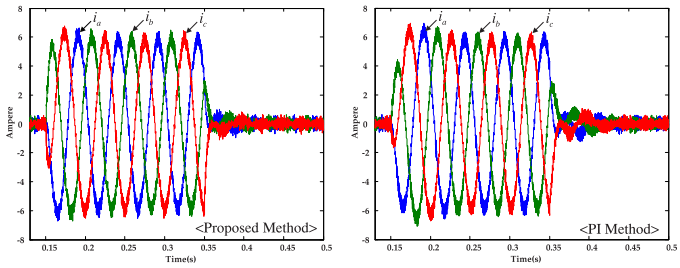

Fig. 6. a-b-c frame current behavior comparison between the proposed method and the PI method at 100 r/min operation for a load torque change.

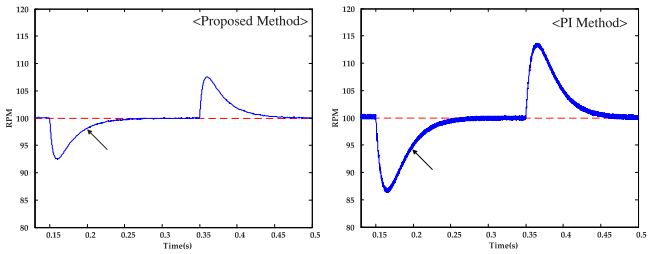

Fig. 7. SPMSM speed regulation performance comparison between the proposed method and the PI method at the 100 r/min operation for a load torque change.

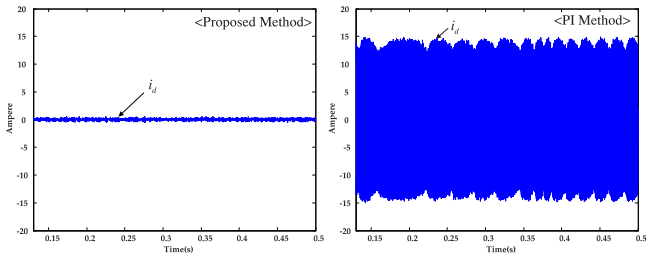

Fig. 8. d-frame current behavior comparison between the proposed method and the PI method at 100 r/min operation for a load torque change.

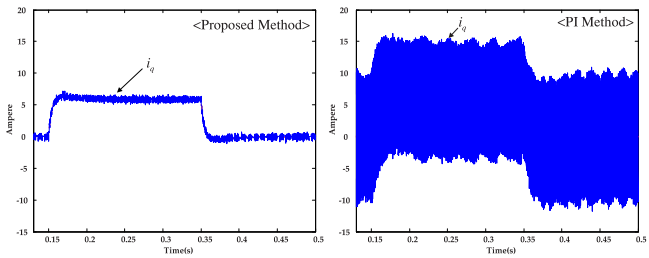

Fig. 9. q-frame current behavior comparison between the proposed method and the PI method at 100 r/min operation for a load torque change.

that the proposed method successfully keeps the closed-loop performance the same as the first simulation result, but the PI method fails. This difference may come from the control gain assignment methods of the two control methods; the proposed method systematically finds control gains by solving an optimization problems of (34)–(40) taking the parameter variations into account, yet the classical cascade PI method does not.

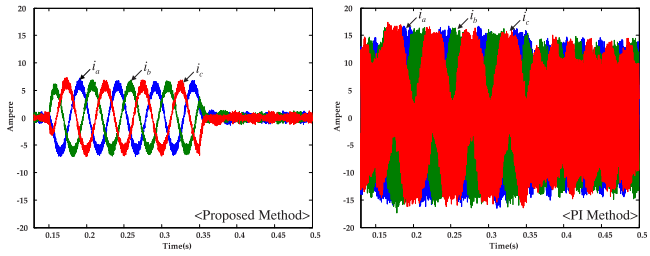

Fig. 10. a-b-c frame current behavior comparison between the proposed method and the PI method at 100 r/min operation for a load torque change.

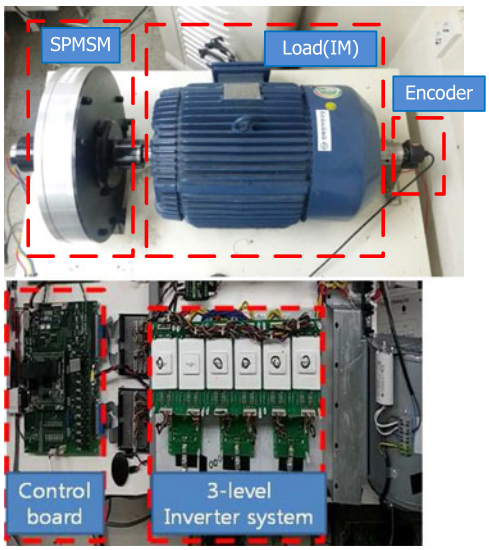

Fig. 11. Hardware setup.

V. Experiments

This section experimentally verifies the efficacy of the proposed method under the same setting of the simulation section, comparing it to the classical cascade PI method. To this end, a 3-kW SPMSM whose rated speed, rated load torque, and peak current are 300 r/min, 95.5 Nm, and 8 A, respectively, was used for this experiment; its true parameter are given the same as (41), and a dc-source voltage $V_{\rm dc}$ was also set the same as the simulation section. The hardware setup is shown in Fig. 11. A digital signal processor TMS320F28335 with a sampling period of $h = 0.1$ ms was utilized to implement the two speed-control algorithms. The implementation of the SVPWM was synchronized with the sampling period for guaranteeing stable operation of the gate drivers. The SPMSM speed information was attained using a rotary incremental encoder, shown in Fig. 11, through the following procedure:

1) calculate the angle of the SPMSM through counting the pulses generated from the encoder;
2) calculate the SPMSM speed by differentiating the angle obtained from the previous step.

The controller parameters of the proposed method and the PI method were left the same as the simulation section, except for the outer-loop tuning parameter. The bandwidth parameter $\omega_{\rm cs}$ of the outer-loop PI controller were set to be $\omega_{\rm cs} = 130$ Hz for

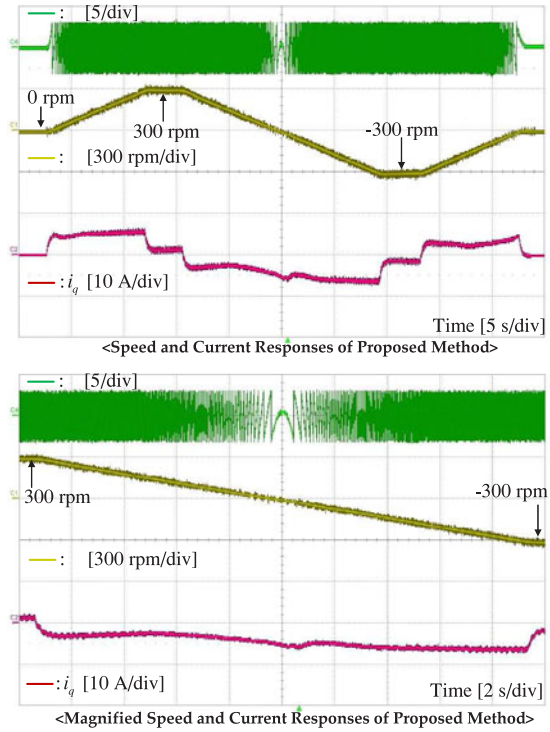

Fig. 12. SPMSM speed tracking performance of the proposed method for a ramp speed reference changing from -300 to 300 r/min.

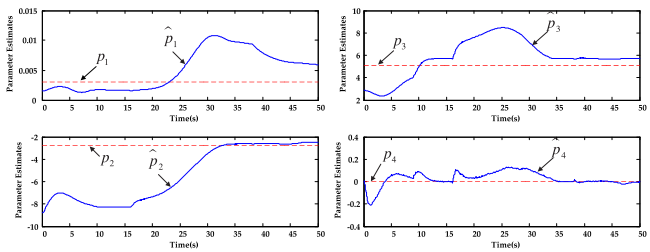

Fig. 13. Behaviors of the parameter estimates.

the best convergence rate with a tolerable overshoot. To constrain the q-frame current, the standard antiwindup algorithm was used for both control methods in their speed-loop PI controllers of (11), (12), (44) where the current limit $i_{q,\max}$ was selected as 8 A.

The first experiment was conducted to show the speed tracking performance of the proposed method with the current behavior in the q-frame under no-load operation where the ramp speed reference changed from -300 to 300 r/min. The resulting speed and current responses are shown in Fig. 12 where the lower panel of this figure enlarges the transient period from -300 to 300 r/min, and Fig. 13 shows the corresponding estimated parameters. The experimental results show that the proposed method successfully drives the PMSM speed to its reference without offset errors as mentioned in Remark 3, and that it provides an acceptable forward/reverse operation mode switching performance.

The second experiment was performed to evaluate the closed-loop performance at 100 r/min under various load operation

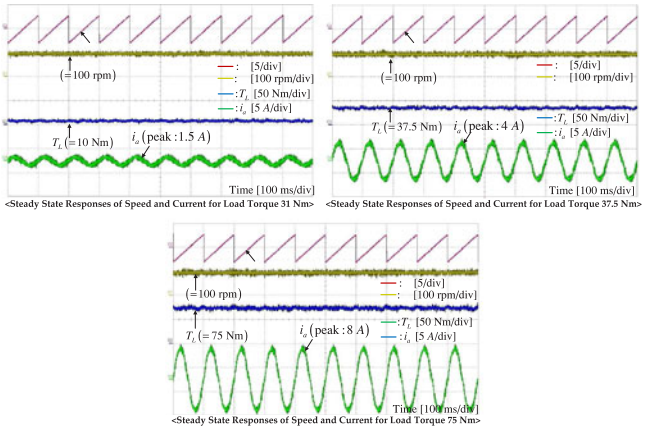

Fig. 14. Speed and current responses in the steady state for load torques $T_L = 10$ Nm, $T_L = 37.5$ Nm, and $T_L = 75$ Nm.

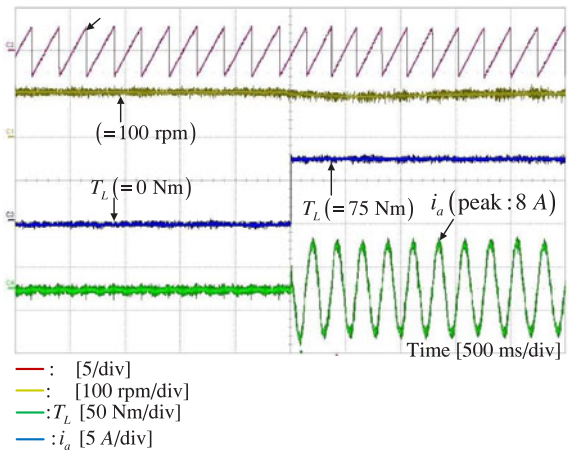

Fig. 15. Speed and current responses in the transient state for a step load torque changing from $T_L = 0$ Nm to $T_L = 75$ Nm.

conditions. The steady-state responses of the speed and the current are shown in Fig. 14 when the load torques $T_L = 10$ Nm, $T_L = 37.5$ Nm, and $T_L = 75$ Nm were applied.

Fig. 15 represents the transient responses of the speed and the current under the step load changing from $T_L = 0$ Nm to $T_L = 75$ Nm.

The transient speed tracking performances between the proposed method and the PI method are compered in the final stage of this experimental study under no-load operation where the ramp speed reference changed from 0 to 100 r/min. Figs. 16–17 show the resulting speed and current responses, which indicate that the proposed method considerably improves the current tracking performance, despite parameter variations.

This result is obvious because the disturbance $\mathbf{Q}(t)\mathbf{p}$ originated from the nonlinearities of SPMSM was systematically treated by the additional control action $\mathbf{Q}(t)\hat{\mathbf{p}}(t)$ of (22). However, the PI method can degrade the closed-loop performance in the transient period because it is impossible to completely cancel the nonlinearities in the SPMSM using F/F compensation terms in the presence of parameter uncertainties.

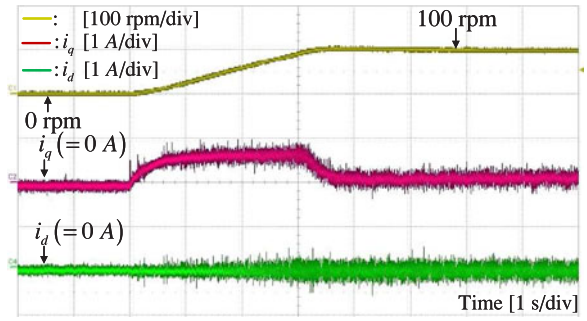

Fig. 16. Speed and dq-frame current responses for the speed reference $\omega_{\mathrm{ref}} = 100$ r/min using the proposed method.

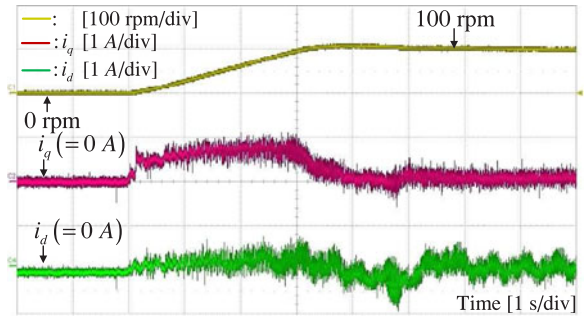

Fig. 17. Speed and dq-frame current responses for the speed reference $\omega_{\mathrm{ref}} = 100$ r/min using the classical PI method.

From these experimental results, we find that the proposed method offers the following two advantages:

1) the proposed method provides a systematic way of choosing the optimal stabilizing control gain, considering the parameter variations;
2) the proposed method maintains satisfactory transient closed-loop performance in real-world implementations.

VI. Conclusion

This article presents two contributions. The first is the development of a control law based on the back-stepping method to stabilize the both the inner and outer loop simultaneously with the offset-free property. The second is the development of a systematic method for finding the optimal, robust control gain value, taking parameter variations into account. Finally, it has been experimentally verified that the proposed method results in satisfactory closed-loop performance in real-world implementations.

References

[1] J. Zhoua and Y. Wang, "Real-time nonlinear adaptive backstepping speed control for a PM synchronous motor," *Control Eng. Practice*, vol. 13, pp. 1259–1269, 2005.

[2] A. Mohammadpour and L. Parsa, "A unified fault-tolerant current control approach for five-phase PM motors with trapezoidal back EMF under different stator winding connections," *IEEE Trans. Power Electron.*, vol. 28, no. 7, pp. 3517–3527, Jul. 2013.

[3] T. Do, S. Kwak, and H. Choi, and J.-W. Jung, "Suboptimal control scheme design for interior permanent-magnet synchronous motors: An

SDRE-based approach," *IEEE Trans. Power Electron.*, vol. 29, no. 6, pp. 3020–3031, Jun. 2014.
[4] J.-C. Hwang and H.-T. Wei, "The current harmonics elimination control strategy for six-leg three-phase permanent magnet synchronous motor drives," *IEEE Trans. Power Electron.*, vol. 29, no. 6, pp. 3032–3040, Jun. 2014.
[5] X. Song, J. Fang, B. Han, and S. Zheng, "Adaptive compensation method for high-speed surface PMSM sensorless drives of EMF-based position estimation error," *IEEE Trans. Power Electron.*, vol. 31, no. 2, pp. 1438–1449, Feb. 2016.
[6] M. Seilmeier and B. Piepenbreier, "Sensorless control of PMSM for the whole speed range using two-degree-of-freedom current control and HF test current injection for low-speed range," *IEEE Trans. Power Electron.*, vol. 30, no. 8, pp. 4394–4403, Aug. 2015.
[7] G.-D. Andeescu, C. Pitic, F. Blaabjerg, and I. Boldea, "Combined flux observer with signal injection enhancement for wide speed range sensorless direct torque control of IPMSM drives," *IEEE Trans. Energy Convers.*, vol. 23, no. 2, pp. 393–402, Jun. 2008.
[8] L. Tang, L. Zhong, M. Rahman, and Y. Hu, "A novel direct torque control for interior permanent-magnet synchronous machine drive with low ripple in torque and flux—A speed-sensorless approach," *IEEE Trans. Ind. Appl.*, vol. 39, no. 6, pp. 1748–1756, Nov./Dec. 2003.
[9] J. Lee, C. Choi, J. Seok, and R. Lorenz, "Deadbeat direct torque control and flux control of interior PMSM with discrete time stator current and stator flux linkage observer," *IEEE Trans. Ind. Appl.*, vol. 47, no. 6, pp. 1749–1758, Jul./Aug. 2011.
[10] I. Boldea and F. Blaabjerg, "Direct torque control via feedback linearization for permanent magnet synchronous motor drives," in *Proc. 13th Int. Conf. Optim. Electr. Electron. Equip.*, 2012, pp. 338–343.
[11] S. Fazeli, H. Zarchi, J. Soltani, and H. Ping, "Adaptive sliding mode speed control of surface permanent magnet synchronous motor using input output feedback linearization," in *Proc. Int. Conf. Electr. Mach. Syst.*, 2008, pp. 1375–1380.
[12] R. Errouissi, M. Ouhrouche, W.-H. Chen, and A. M. Trzynadlowski, "Robust cascaded nonlinear predictive control of a permanent magnet synchronous motor with antiwindup compensator," *IEEE Trans. Ind. Electron.*, vol. 59, no. 8, pp. 3078–3088, Aug. 2012.
[13] K. Jezernik, J. Korelic, and R. Horvat, "PMSM sliding mode FPGA-based control for torque ripple reduction," *IEEE Trans. Power Electron.*, vol. 28, no. 7, pp. 3549–3556, Jul. 2013.
[14] M. L. Corradini, G. Ippoliti, S. Longhi, and G. Orlando, "A quasi-sliding mode approach for robust control and speed estimation of PM synchronous motors," *IEEE Trans. Ind. Electron.*, vol. 59, no. 2, pp. 1096–1104, Feb. 2012.
[15] S. Chai, L. Wang, and E. rogers, "A cascade MPC control structure for a PMSM with speed ripple minimization," *IEEE Trans. Ind. Electron.*, vol. 60, no. 8, pp. 2978–2987, Aug. 2013.
[16] M. Preindl and S. Bolognani, "Model predictive direct speed control with finite control set of PMSM drive systems," *IEEE Trans. Power Electron.*, vol. 28, no. 2, pp. 1007–1015, Feb. 2013.
[17] Y.-S. Kung and M.-H. Tsai, "FPGA-based speed control IC for PMSM drive with adaptive fuzzy control," *IEEE Trans. Power Electron.*, vol. 22, no. 6, pp. 2476–2486, Nov. 2007.
[18] N. T.-T. Vu, D.-Y. Yu, H. H. Choi, and J.-W. Jung, "T–S fuzzy-model-based sliding-mode control for surface-mounted permanent-magnet synchronous motors considering uncertainties," *IEEE Trans. Ind. Electron.*, vol. 60, no. 10, pp. 4281–4291, Oct. 2013.
[19] H. H. Choi, N. T.-T. Vu, and J.-W. Jung, "Digital implementation of an adaptive speed regulator for a PMSM," *IEEE Trans. Power Electron.*, vol. 26, no. 1, pp. 3–8, Jan. 2011.
[20] M. Karabacak and H. I. Eskikurt, "Speed and current regulation of a permanent magnet synchronous motor via nonlinear and adaptive backstepping control," *Math. Comput. Model.*, vol. 53, pp. 2015–2030, 2011.
[21] S.-K. Kim, K.-G. Lee, and K.-B. Lee, "Singularity-free adaptive speed tracking control for uncertain permanent magnet synchronous motor," *IEEE Trans. Power Electron.*, vol. 31, no. 2, pp. 1692–1701, Feb. 2016.
[22] G. Foo and M. Rahman, "Direct torque and flux control of an IPM synchronous motor drive using a backstepping approach," *IET Electr. Power Appl.*, vol. 3, pp. 413–421, 2008.
[23] J. Yu, P. Shi, W. Dong, B. Chen, and C. Lin, "Neural network-based adaptive dynamic surface control for permanent magnet synchronous motors," *IEEE Trans. Neural Netw. Learn. Syst.*, vol. 26, no. 3, pp. 640–645, Mar. 2015.
[24] M. A. Rahman, D. M. Vilathgamuwa, M. N. Uddin, and K.-J. Tseng, "Nonlinear control of interior permanent-magnet synchronous motor," *IEEE Trans. Ind. Appl.*, vol. 39, no. 2, pp. 408–416, Mar./Apr. 2003.
[25] M. Morawiec, "The adaptive backstepping control of permanent magnet synchronous motor supplied by current source inverter," *IEEE Trans. Ind. Inf.*, vol. 9, no. 2, pp. 1047–1055, May 2013.
[26] M. Kadjoudj, M. E. H. Benbouzid, C. Ghennai, and D. Diallo, "A robust hybrid current control for permanent magnet synchronous motor drive," *IEEE Trans. Energy Convers.*, vol. 19, no. 1, pp. 109–115, Mar. 2004.
[27] S.-S. Ke and J.-S. Lin, "Sensorless speed tracking control with backstepping design scheme for permanent magnet synchronous motors," in *Proc. IEEE Conf. Control Appl.*, 2005, pp. 487–492.
[28] S. Boyd, L. E. Ghaoui, E. Feron, and V. Balakrishnan, *Linear Matrix Inequalities in System and Control Theory*. Philadelphia, PA, USA: SIAM, 1994.
[29] H. K.Khalil, *Nonlinear Systems*, 3rd ed. New York, NY, USA: Prentice-Hall, 2002.

Seok-Kyoon Kim received the B.S. degree from the Seoul National University of Science and Technology, Seoul, Korea, in 2004, and the Ph.D. degree in electrical engineering from the Korea University, Seoul, Korea, in 2014.

He is currently working for the Vehicle Component Technology Center, LG Electronics as a Senior Research Engineer since 2015. His research interests include passivity-based control, nonlinear adaptive control, power system stabilization, and tracking and stabilization problems of power electronic applications such as power converters and motor drive.

June-Seok Lee (S'11–M'15) received the B.S., M.S., and Ph.D. degrees in electrical and computer engineering from Ajou University, Suwon, Korea, in 2011, 2013, and 2015, respectively.

Since 2015, he has been with the Korea Railroad Research Institute, Uiwang, Korea. His research interests include grid-connected systems, multilevel inverter, and reliability.

Kyo-Beum Lee (S'02–M'04–SM'10) received the B.S. and M.S. degrees in electrical and electronic engineering from Ajou University, Suwon, Korea, in 1997 and 1999, respectively. He received the Ph.D. degree in electrical engineering from the Korea University, Seoul, Korea, in 2003.

From 2003 to 2006, he was at the Institute of Energy Technology, Aalborg University, Aalborg, Denmark. From 2006 to 2007, he was with the Division of Electronics and Information Engineering, Chonbuk National University, Jeonju, Korea. In 2007, he joined the School of Electrical and Computer Engineering, Ajou University, Suwon, Korea. He is an Associate Editor of the IEEE TRANSACTIONS ON POWER ELECTRONICS, *Journal of Power Electronics*, and *Journal of Electrical Engineering and Technology*. His research interests include electric machine drives, renewable power generations, and electric vehicles.